Ceramics International 51 (2025) 72–84

Contents lists available at ScienceDirect

Ceramics International

journal homepage: www.elsevier.com/locate/ceramint

Influence of the lemon (*Citrus Limon L.*) juice amount on the green synthesis of CuO nanoparticles: Characterization, stability and thermal conductivity

Meriem Jebali [a,b], Ana Isabel Gómez-Merino [b,*], Gianpiero Colangelo [a]

[a] Department of Engineering for Innovation, University of Salento, Lecce, 73100, Italy
[b] Department of Applied Physics II, University of Málaga, Málaga, 29071, Spain

ARTICLE INFO

Handling Editor: Dr P. Vincenzini

1. Introduction

Green synthesis has focused much attention because reduces toxic and unhealthy products to the environment released by physicochemical techniques. Green synthetic processes are more cost-effective and boost the utilization of biological substances such as algae, fungi, bacteria and fundamentally plant-derived extracts. These materials are known as biogenic nanomaterials [1]. Plant-derived nanopowders could be prepared by precursors commonly found in plant leaves, seeds, peels, stems, flowers, fruits, or juices [1–3].

Recently, the use of *Citrus Limon* L. in the green synthesis of metal oxides has marked significant progress due to the abundant, non-toxic characteristics of lemon juice to produce high-quality metal oxides, minimizing environmental impact and improving the safety and effectiveness of the produced materials. The lemon juice is renowned for its high content of flavonoids, polyphenols, and carboxylic acids. All these biomolecules can function as stabilizers and/or complexing agents, influencing various properties, such as the size and morphology of the metal oxide nanoparticles [4,5].

Copper is an essential micronutrient in human, animals and plants in different oxidation states (Cu^{+}, and Cu^{2+}), which develops many functions of human immune cells. Copper-based materials have attracted researcher's attention because of their use in various technologies. They are valued for their antimicrobial properties, making them suitable for medical purposes and water purification treatments [6–8]. Other applications involve textile industries, biosensors, superconductors, catalysts, heat exchangers as well as environmental cleanliness [9,10]. Currently, the extract of leaf-plant is used in the majority of the CuO green preparation with the lack of synthesis mediated by other plant derivatives [11]. The biosynthesis of CuO NPs has usually been performed by using plant leaves and $CuSO_4$ or $Cu(NO_3)_2$ as precursor salts [9–11]. Other researchers have prepared spherical CuO NPs by adding filtered lemon extract [12] and lemon juice/polyvinylpyrrolidone (PVP) as a stabilizer in a 1:1 ratio [13]. However, future challenges related to the optimization of the synthesis process to control size, shape and nanomaterial quality are needed due to the diversity of phytochemicals contained in these extracts [14]. The common parameters in the synthesis of CuO NPs are plant extract and salt precursor concentrations, mixture heating temperature, time of stirring and annealing temperature. Generally, in the plant-mediated synthesis and more specifically in the lemon juice (LJ) green synthesis the proportion LJ/salt precursor reported is the stochiometric ratio 1:1 [11,15]. In another work [16], lead hexaferrite is synthesized by utilizing cherry juice at different volumes and calcination temperatures. The best powder quality in terms of aggregation and size has been reached with higher volumes of cherry juice. Based on these findings, further significant research on the green synthesis of nanoparticles under different parameters is needed to enable industrial production of environmentally friendly nanomaterials [7,8].

Another research gap is related to the applications of CuO green synthesis in other fields different from biomedical industries. The optimization of green synthesis to achieve high disaggregated and small NPs is envisioned to be critical for the future of nanofluid research in heat transfer applications through the thermal conductivity enhancement of the liquid phases [11,17]. CuO NPs are increasingly used in nanofluids due to their excellent thermal conductivity, which significantly improves the heat transfer performance of the fluid. However, the parameters that influence the effective thermal conductivity of nanofluids

* Corresponding author.
E-mail address: aimerino@uma.es (A.I. Gómez-Merino).

https://doi.org/10.1016/j.ceramint.2024.10.330
Received 2 May 2024; Received in revised form 6 October 2024; Accepted 22 October 2024
Available online 30 October 2024

have been a matter of wide controversy over the years, which may affect the growth of nanofluids in the industrial trade. Although the increment of NP concentration always leads to an increase of nanofluid TC diverse research findings have been reported about the dependency of k_{eff} with particle diameter, d_p. Large number of investigations [18] have found an increase of the TC with particle size reduction, which boosts at higher temperatures and particle concentration, while other works have detected an inverse reduction of TC with d_p [18,19]. Therefore, different studies have reported contradictory effects of particle diameter on thermal conductivity even for the same particle, concentration, temperature and base liquid. The disagreement reported in the experimental works could emerge from the lack of wide-ranging data on characteristic parameters affecting the effective thermal conductivity of nanofluids. Therefore, further measures of k_{eff} in wide ranges of temperature and concentration, particle morphology (size and shape) characterization, size distribution in the nanofluid, hosting fluid properties, liquid phase pH, surfactant type and stability procedures are recommended to address these experimental conflicts. The use of various TC measurement techniques has also raised inconsistencies in several experimental studies on k_{eff} [18,19].

Apart from facilitating the suspension stability particle size and shape also affect the heat transfer mechanism of the dispersion. Maheshwary et al. [20] have conducted an extensive experimental study to evaluate the effect of particle size and shape on the effective thermal conductivity (k_{eff}) of TiO_2/water nanofluids at temperatures ranging from 30 °C to 80 °C. They have found that reducing particle size k_{eff} enhances. Cubic-shaped NPs provide the highest k_{eff}, followed by rod-like and spherical shapes. However, Timofeeva et al. [21] have determined k_{eff} of the $Al_2O_3/EG-H_2O$ suspensions of different particle shapes - blades, platelets, cylinders and bricks. Blade-like nanoparticles display the highest k_{eff} improvement followed by platelet, cylinder and brick-like NPs. In all the reported TC measurements, spheroidal particles exhibit higher enhancement than spherical particles [18,19]. In many studies, the experimental and theoretical thermal conductivities of dispersions exhibit discrepancies. In many cases, this is due to the lack of particle dimensions in several theoretical approaches. Contradictory conclusions have been obtained considering the different nanofluid heat transfer mechanisms such as diffusive phonon transport, liquid layering, particle clustering and Brownian motion [22–25]. To shed light on these inconsistencies, systematic investigations with uniform procedures for the NP synthesis, TC measures, particle morphology characterization techniques and stability of dispersions are recommended [18,19]. However, other theoretical approaches considering the interfacial layer effect [26] and Brownian motion, agglomeration of particles and liquid nanolayers [27] have successfully been applied. In both theories, the particle and particle aggregate diameters and the thickness of the liquid boundary layer are relevant parameters.

The stability of suspensions is a crucial factor for reproducible TC measurements and is a challenge for the industrial application of colloidal dispersions. Surfactants play an important role in facilitating suspension stability by reducing the solid/liquid interface tensions and controlling the size and agglomeration of nanoparticles, which also provides stabilizing effects [28,29]. Among the anionic surfactants, the most extensively used are sodium dodecyl benzene sulfonate (SDBS) and sodium dodecyl sulfate (SDS).Pavithra et al. [30] have investigated the impact of SDS and polyvinylpyrrolidone (PVP) surfactants on the thermal conductivity of CuO/water-based nanofluids. The use of 0.4 wt% SDS and PVP in a 0.5 vol% CuO suspension leads to increases in thermal conductivity of 38 % and 34 %, respectively. Arasu et al. [31] have revealed that SDS led to the formation of more stable nanofluids, resulting in a substantial thermal conductivity enhancement of 29.6 % at 60 °C and a concentration of 0.1 wt%, in contrast to the 2.1 % improvement achieved with SDBS at the same mass concentration.

To the best knowledge of the authors, no research has been done regarding the influence of the *LJ/Metal salt* (L/M) ratio on the size, shape and quality of CuO plant mediated synthesis. In this study, the effect of three L/M ratios on the morphology and thermal conductivity of CuO plant-mediated synthesis was evaluated for the first time. The work was structured as follows: In section 3.1, an overall description of the three synthesis processes was set up. In section 3.2, a complete characterization of the three synthesized CuO NPs through electron microscopy (SEM, TEM), FTIR, XRD and TGA/DTA was conducted. In section 3.3, the stability of the three CuO NPs dispersed in EG/DW (60:40) was accomplished by dynamic light scattering (DLS) and zeta potential measurements. The fact of having three NPs with the same chemical nature but different sizes and powder qualities in terms of disaggregation made it possible to perform a comparative study of the experimental thermal conductivities under uniform standards. Additionally, these experimental TC data of the three CuO-EG/DW nanofluids were compared with those obtained from two mathematical models. These results are presented in section 3.4.

2. Experimental setup, materials and methods

2.1. Synthesis of copper oxide nanoparticles

Copper oxide nanoparticles were prepared as it is schematically reported in Fig. 1 following similar procedures already reported [13,32]. Copper (II) nitrate trihydrate ($Cu(NO_3)_2{\cdot}3H_2O$) obtained from Sigma-Aldrich, with a purity of 99 %, was utilized in its as-received state without additional purification. Lemon fruits underwent meticulous cleaning, then, they were cut, squeezed and homogenized through magnetic stirring for 30 min. The juice was filtered with Whatman No. 1 paper to remove solid particulates. Copper oxide nanoparticles were synthesized through a two-step process involving the dissolution of Copper (II) nitrate trihydrate in deionized water, followed by the addition of the lemon juice in different ratios Lemon/Metal salt (L/M). The synthesis took place at 80 °C, leading to an exothermic oxidation reaction and the formation of dark brown precipitates (step 1). After cooling, the nanoparticles underwent washing cycles with deionized water and were subsequently dried and calcined at 750 °C for 120 min (step 2). In this paper three ratios were explored L/M = 0.33; L/M = 1 and L/M = 3.

2.2. Preparation of CuO nanofluids

CuO nanofluids were prepared through a two-step method. Firstly, the powders were weighed by using an AE-163 electronic 10^{-4} g precision balance (Mettler-Toledo, Columbus, OH, USA). Then, they were dispersed in the base fluid Ethylene glycol/Water 60:40 at 0.2 % volume fraction. To achieve uniform dispersion, the mixtures underwent 30 min magnetic stirring at 600 rpm, then, sodium dodecyl sulfate (SDS) 1.5 %, wt/v, Sigma-Aldrich 99 % purity, was incorporated, followed by ultrasonication at 40 kHz, with HF-peak out of 72 W, according to the recommendations of Kaggwa et al. [33]. The time of sonication was also assessed from 0 to 180 min.

2.3. Characterization equipment

Fourier Transform Infrared (FT-IR) measurements were performed using a PerkinElmer Frontier MIR/FIR spectrophotometer in KBr pellets in the interval of 400–4000 cm^{-1}. X-ray diffraction (XRD) spectra were recorded with a D8 Advance Bruker diffractometer CuKα radiation (λ = 1.5418 Å) from 20° to 80° with a rate of 0.002 2θ/s. Diffractograms were treated with the X'pert High Score Plus software. The surface morphology of the powder was scanned by Transmission Electron Microscopy TEM (JEOL JEM-1400) with an accelerating voltage of 120 kV, at various magnifications with a connected energy dispersive X-ray spectroscopy (X-EDS) accessory and a high-resolution Gatan ES1000W camera. X-ray Photoemission Spectroscopy (XPS) spectra were recorded in a PHI Model 5700 X-Ray MultiTechnique System Photoelectron Spectrometer. Xray source Mg 1253.6 eV std at 300.0 W. Spectra were obtained using an ion beam charge neutralization diameter of 720.0 μm.

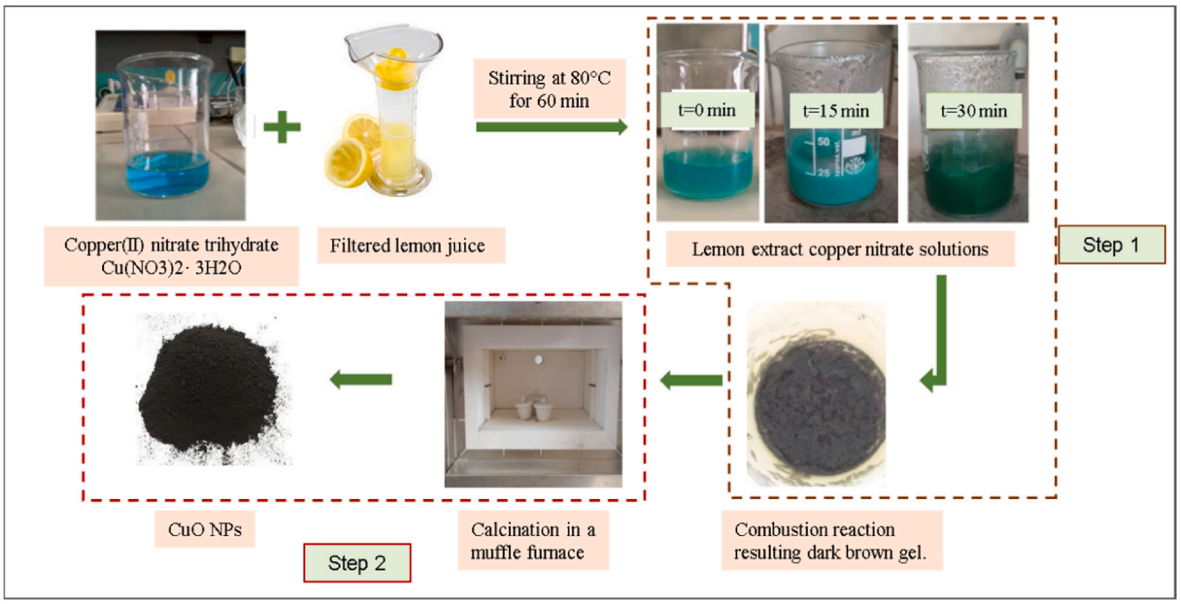

Fig. 1. Scheme of the green synthesis of copper oxide nanoparticles. (For interpretation of the references to colour in this figure legend, the reader is referred to the Web version of this article.)

All the spectra were performed on the brown gel after combustion reaction (step 1 in Fig. 1). Thermogravimetric and differential thermal analysis (TG/DTA) was carried out using a PerkinElmer Thermal gravimeter STA 6000 thermal analyzer from 25 °C to 750 °C with a heating rate of 10 °C/min under Nitrogen atmosphere. Both the average particle diameter, obtained by dynamic light scattering (DLS), and the zeta potential of the CuO-based nanofluid clusters dispersed in EG/W 60:40 was estimated with the Litesizer DLS 500 equipment (Anton Paar, GmbH, Graz, Austria). DLS sensitiveness is under 1 nm. It is provided with three backscatter angles, 15°, 90°, or 175° with small times of measures, a laser light source of 658 nm and 40 mW and an integrated Peltier-type temperature control device with an accuracy of 0.01 °C. Particle concentration was prepared under 22 mg/ml. All measurements were done three times for every sample. The thermal conductivity of the CuO-based nanofluids was assessed using the KD2 Pro thermal properties analyzer (Decagon Devices, Inc, Pullman, WA, USA), adhering to the ASTM D5334 standards and IEEE 442–1981 regulations. This analyzer employs the Transient Hot Wire method (THW) for thermal conductivity

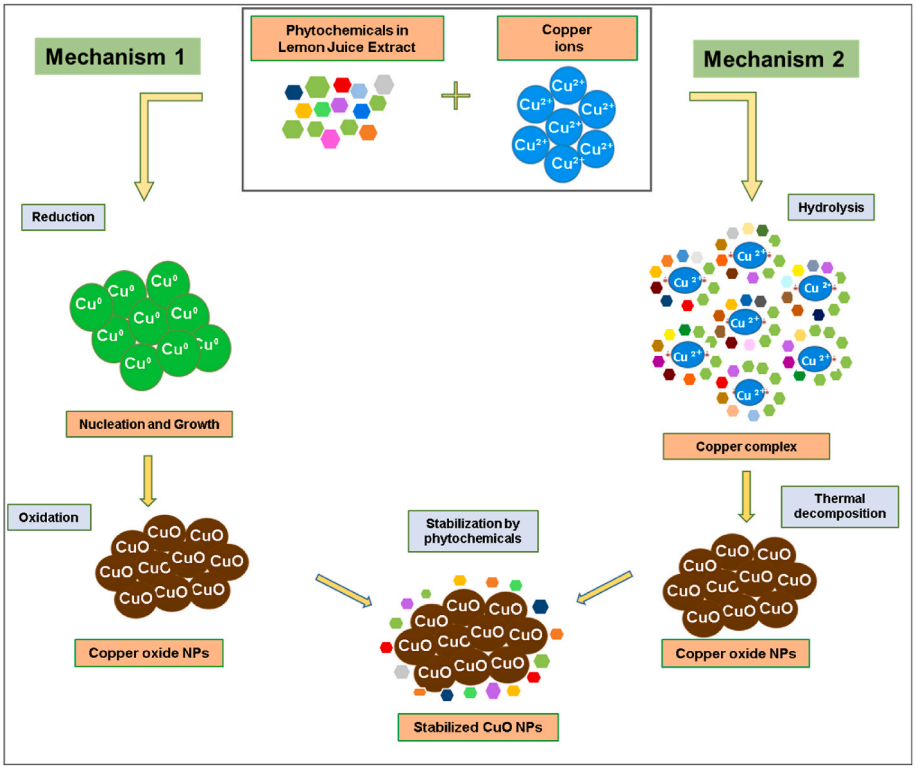

Fig. 2. Scheme of the two proposed mechanisms for the green formation of CuO nanoparticles using lemon extract. (For interpretation of the references to colour in this figure legend, the reader is referred to the Web version of this article.)

measurements, featuring a reading unit and a single-needle sensor with a 1.27 mm diameter and 60 mm length. The sensor was vertically immersed into the nanofluid sample within a cylindrical cell placed in a temperature-controlled bath. The thermal conductivity tests were conducted thrice over a temperature range of 20–60 °C.

3. Results and discussions

3.1. Mechanism of the green synthesis of CuO

To elucidate the mechanism by which lemon juice can be used to form metal oxides, the literature presents two hypotheses (see Fig. 2). The first hypothesis suggests that the formation of CuO NPs occurs due to a change in the oxidation state of the Cu^{2+} ions of the precursor salt to zero-valent copper (Cu^0). Subsequently, the metallic copper nanoparticles undergo oxidation and transform into CuO NPs through interaction with the atmospheric oxygen. This transition results in a change in the oxidation state of copper returning it to its original state but in a different form. The preparation of CuO NPs through this mechanism involves three stages: *nucleation, growth*, and *stabilization*. In the stabilization step, the plant's extra bio-macromolecules create a protective shield and prevent agglomeration [7,9,34,35].

The second proposed mechanism postulates that the oxidation state of copper remains unchanged during the green synthesis of CuO nanoparticles using the plant extract. This mechanism involves the formation of coordination complexes between the copper ions and various phytochemicals present in the plant extract. These phytochemicals act as ligands and donate their lone pairs of electrons, leading to the formation of stable complexes with the copper ions. The presence of these phytochemicals stabilizes the reaction mixture and prevents further oxidation or reduction of the copper species. This mechanism of the green synthesis of CuO NPs using plant extract could be divided into three steps: *hydrolysis, complexation*, and *thermal decomposition* [36].

To shed light on the mechanism that led to the CuO synthesis the three dark brown gels (step 1), deriving from the three proportions of lemon juice/precursor salt (L/M) above mentioned, were analyzed by X-ray Photoemission Spectroscopy (XPS). Fig. 3 shows the corresponding 2p and O1 spectra of the three pastes named as L/M = 0.33; L/M = 1 and L/M = 3, according to the ratio of L/M ratio employed in the synthesis.

In Fig. 3 it can be appreciated the 953.5 eV band corresponding to Cu $p_{1/2}$ valence state of CuO and the Cu $2p_{3/2}$ values, 932.7 eV and 934.6 eV, which are characteristics of reduced Cu (Cu^0/Cu^I), and Cu^{II} species, respectively. Although distinguishing Cu^I and Cu^0 species may, in principle, be intricate from these spectra, the high surface concentration of O^{2-} and OH^- species, as revealed by the O1s spectrum (Fig. 3b), suggests that the pastes are composed of Cu_2O and $Cu(OH)_2$ and organic components, such as carboxylate species [37]. Deconvolution of peaks resulted in the corresponding Cu_2O/$Cu(OH)_2$ ratios (Fig. 3a). As it can be observed, the proportion of Cu_2O increases with the lemon juice addition, which agrees with the higher solubility of Cu^{II} oxide/hydroxide in the presence of carboxylic acids, such as citric acid [38]. Similar XPS spectra of CuO have been described by other authors [39]. According to the XPS bands displayed in Fig. 3, there is no trace of Cu^0 in any of the three gels. Therefore, from this evidence it could be inferred that mechanism 2 more convincingly explained the role of the lemon juice phytochemicals in the green synthesis of CuO.

3.2. Characterization of the powders

3.2.1. FTIR analysis

As it can be seen from the diagrams shown in Fig. 4a, the FTIR Spectra of the sample's L/M = 0.33; L/M = 1 and L/M = 3 calcined at 750 °C were similar. The absorption bands at 3344 cm^{-1} were related to the O–H stretching vibration of physiosorbed water molecules, of alcohols or plant phenolics. The band observed at 1624 cm^{-1} was attributed to the C=C stretching vibration of the aromatic rings, and the functional groups present in the phytocompounds from the plant extract. The bands in the region 1327 cm^{-1} and 1127 cm^{-1} could be assigned to the stretching vibration of carboxylic acids and amino functional groups, whereas the peak at 1010 cm^{-1} corresponded to C-O bond of the flavonoids. The three FTIR spectra displayed absorption bands at 474 cm^{-1} and 587 cm^{-1} for the Cu-O band. The FTIR study of the three powders showed the formation of CuO and the presence of organic residue coming from the lemon juice, which increased with the amount of lemon juice used in the synthesis. These results are consistent with previously reported works of CuO nanoparticles synthesized using different fruit extracts [14,15,40].

3.2.2. XRD difractograms

The Crystallinity of the three samples was investigated by XRD measurements to confirm the formation of CuO nanoparticles. The XRD pattern of the prepared nanoparticles with the three L/M ratios are shown in Fig. 4b. As it can be seen, when the ratio is L/M = 0.33 or L/M = 1, the XRD patterns of the samples exhibits diffraction peaks corresponding to lattice planes of (110), (11-1), (200), (11-2), (20-2), (112), (020), (021), (202), (11-3), (02-2), (310), (113), (311), (004) and (22-2) of the monoclinic structure of CuO (JCPDS No. -03-065-2309) [40–42]. No additional peaks from impurities were detected for these two samples, which confirms the high purity and the efficiency of the lemon extract for synthesizing CuO NPs without the presence of other crystalline phases. However, for the highest L/M = 3 ratio, CuO was formed with the existence of new peaks in the XRD pattern at 29.59°, 36.36°, 42.23°, 73.41° and 77.32°, which are characteristic peaks for the cubic structure of Cu_2O, as illustrated in Fig. 4b. It was discussed in previous works that the existence of impurities could be attributed to the lack or excess of the L/M ratio [18]. In this work, the excess of lemon juice

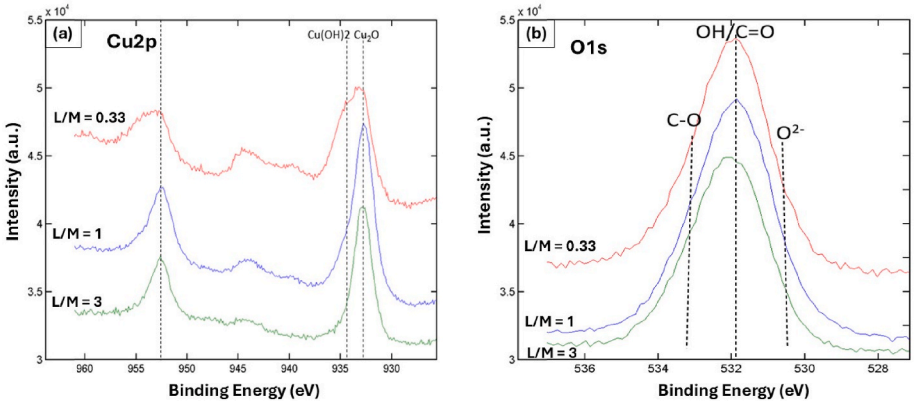

Fig. 3. X-ray Photoemission Spectroscopy (XPS) spectra of the three CuO nanopowders. (a) Cu2p and (b) O1s.

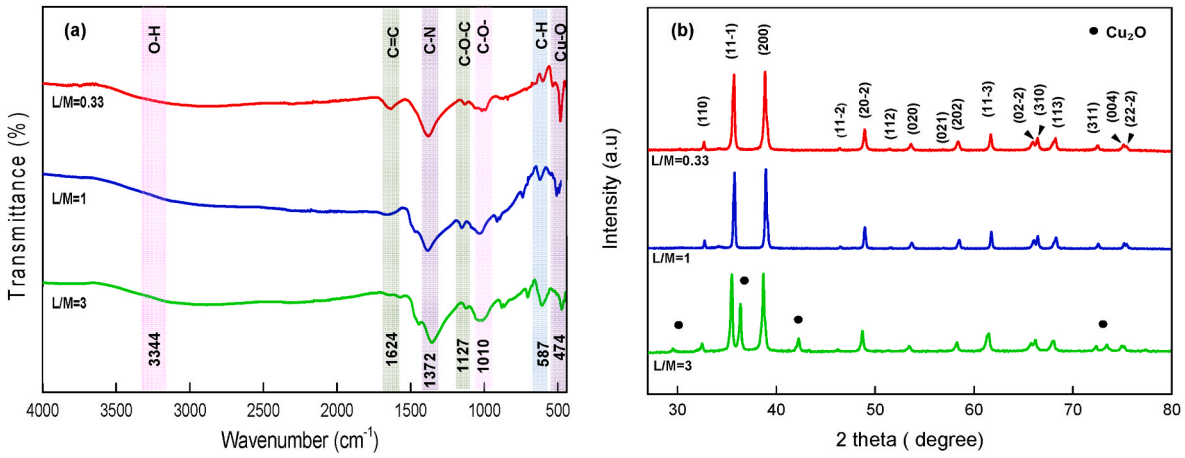

Fig. 4. (a) FTIR and (b) XRD spectra of the three powders.

caused the reduction of Cu^{2+} to Cu^{+} and then Cu_2O was synthesized as impurity. According to the XRD pattern, it can be concluded that in the synthesis of pure CuO a low or stoichiometric amount of lemon juice was required. The smallest average crystalline size of around 31 nm was observed for the sample L/M = 0.33 and the average crystalline size increased successively for higher lemon juice amount to be 35 nm for the sample L/M = 1 and 40 nm for the sample L/M = 3. Therefore, when the amount of LJ increased both the intensity of the diffraction peaks and crystalline size increased.

3.2.3. TG/DTA analysis

Fig. 5 represents the TGA/DTA of the as-prepared CuO (the gel form) before the calcination process (step 1). As it is shown in Fig. 5, the first weight loss of about 5 % was observed at 25–180 °C with an endothermic peak that could be attributed to the desorption of the water molecules absorbed on the gel surface. In the temperature range from 180 °C to 300 °C, the second weight loss of about 18 % occurred due to the gel decomposition [42]. The last weight loss was recorded from 300 °C to 800 °C accompanied by exothermic peaks seen in the DTA curve and it could be related to the loss of the residual organic compounds, the combustion of the copper nitrate and the thermal decomposition of amorphous $Cu(OH)_2$ into the crystalline CuO form [41,42].

3.2.4. Electron microscopy

The SEM micrographs (a-b-c) of the sample's L/M = 0.33, L/M = 1 and L/M = 3 is exhibited in Fig. 6. They show agglomerated spheroidal shape particles. The TEM images shown in Fig. 6d-e-f of the three powders exhibit similar agglomerated nanoparticles of platelet or spheroidal shape. Although the L/M = 0.33 shows a more disaggregated aspect powder. The histograms with a Gaussian distribution of the particle size for the three powders confirms that the CuO sample microstructures depend on the LJ addition. In the presence of a small amount of lemon juice L/M = 0.33, the particle had the smallest size distribution (10–40 nm) with an average diameter of about 27 nm. The sample L/M = 3, prepared with a higher amount of lemon juice, had the largest particle size distribution (23–64 nm) with an average diameter of about 31 nm. When the LJ was in the stoichiometric quantity (L/M = 1) the particle size distribution was in the range (12–68 nm) with an average diameter of about 37 nm. Fig. 6(g and h-i) shows the XEDS compositional spectra of the three above-mentioned powders. The L/M = 0.33 sample presents the energy of the Cu peak at 24 eV and 22 eV, respectively, vs. 14 eV and 9 eV of the sample L/M = 1 and 12 eV and 6 eV of the sample L/M = 3. It is also seen how the increase in the amount of lemon juice produced higher quantities of atoms related to the presence of organic compounds such as K and P. These results agree with those obtained by other researchers [19] and with the XPS, FTIR and XRD spectra. All the characterization techniques above discussed validated the L/M = 0.33 CuO nanopowder as the best quality in terms of purity and morphology.

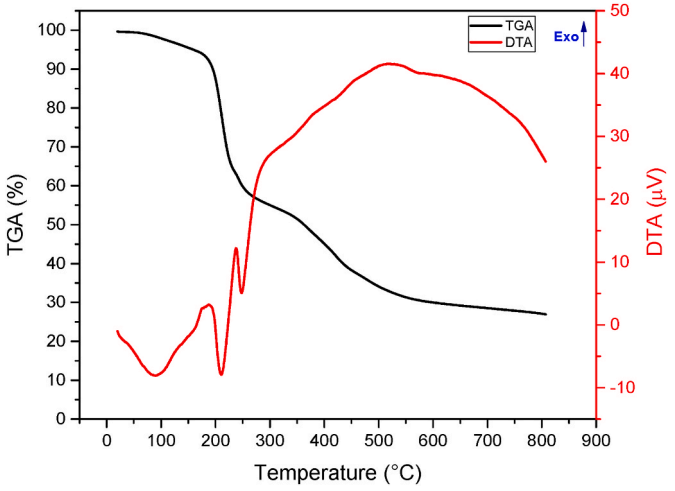

Fig. 5. TG/DTA analysis of the as-prepared CuO gel.

3.3. Stability of nanofluids

The characteristics and the nature of CuO dispersed in EG/W 60:40, even at low concentration (0.2 vol%), required analyzing their stability especially for heat transfer applications. This was accomplished by using DLS measurements and sedimentation tests [43,44].

3.3.1. Ultrasonication time and surfactant effect

DLS measurements can be influenced by a variety of parameters including nanoparticle concentration, shape and morphology, base fluid composition, surfactants, ultrasonication time, temperature, and suspension viscosity. The ultrasonication process induces mechanical vibrations, promoting air bubble formation, which contributes to stabilize nanofluid suspensions. The hydrodynamic diameter (HD) of the CuO NPs dispersed in EG/W 60:40, with and without surfactant for different ultrasonication times are shown in Fig. 7a. At ultrasonication time t_{sn} = 0 min (after stirring only), the hydrodynamic diameter of the samples without surfactant S1, S3 and S5 were about 518.0; 564.1; 647.9 nm, respectively, vs. 313.4; 360.4; 439.6 nm, for the samples with SDS 1,5 wt % S2, S4 and S6, respectively, as it is shown in Fig. 7a. These samples reduced the HDs 39.50 %, 36.11 % and 32.15 %, respectively. When the ultrasonication process started, the HD of the clusters decreased rapidly.

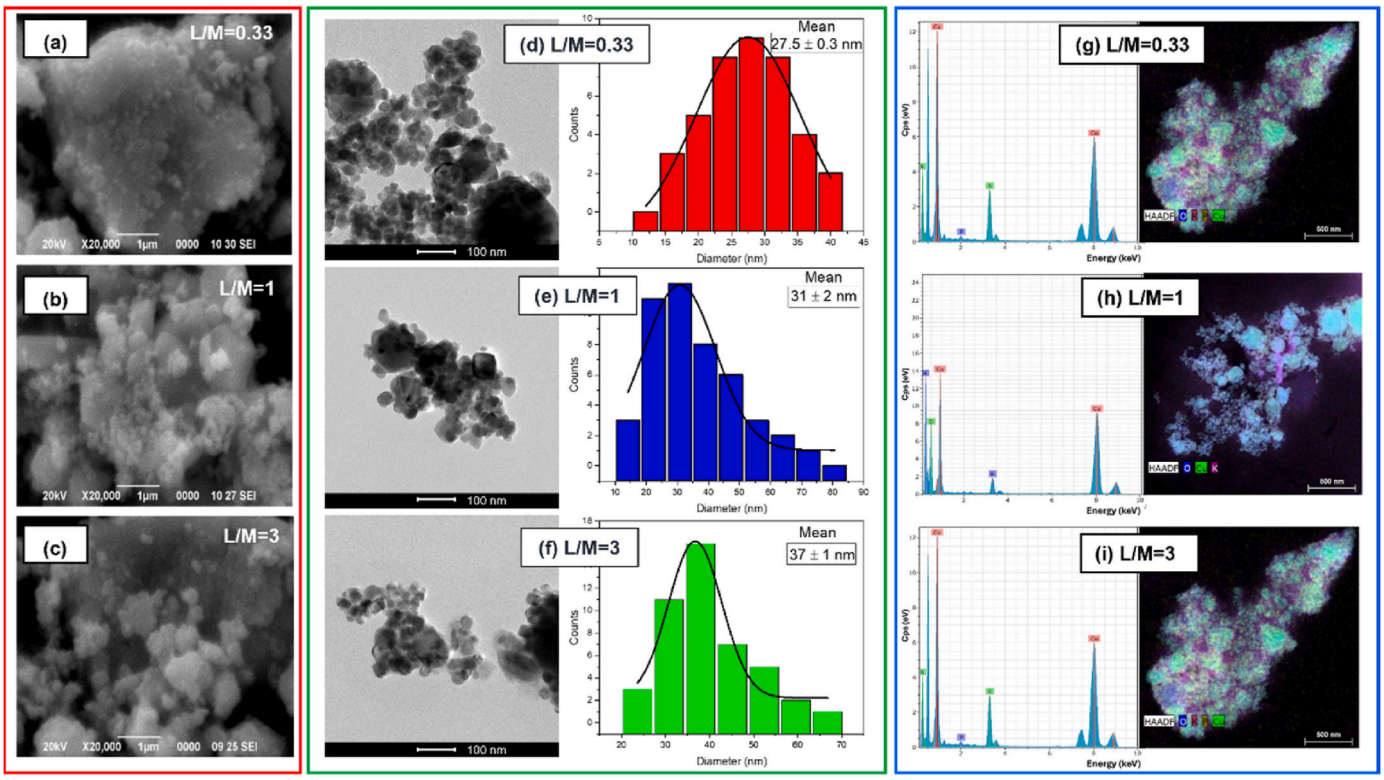

Fig. 6. (a,b,c) Scanning electron images (SEM) of the three powders, (d,e,f). Transmission electron micrographs (TEM) and particle diameter distribution of the three powders. (g,h,i) L/M = 0.33, L/M = 1 and L/M = 3. X-EDS spectra and High-angle annular dark-field (HAADF) images of the three powders.

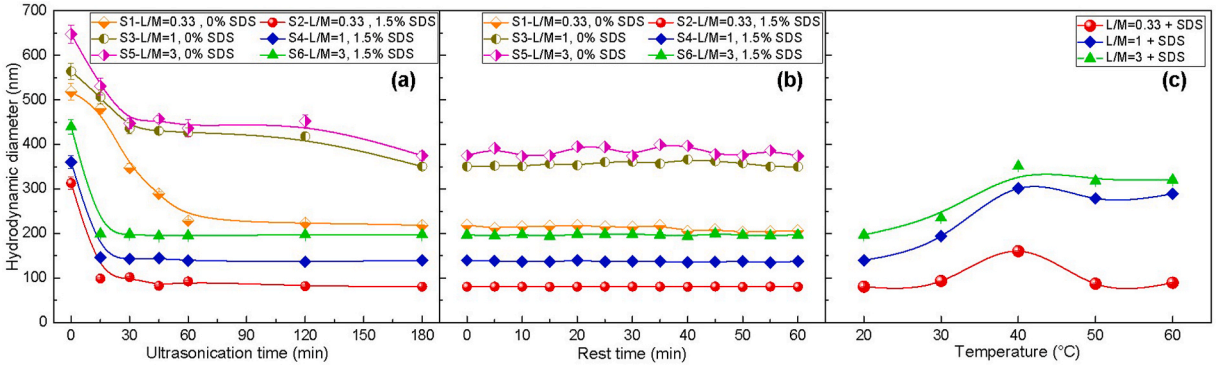

Fig. 7. (a) Hydrodynamic diameter (HD) of CuO nanoparticles dispersed in EG/W 40:60 at different ultrasonication duration. The effect of the surfactant is also shown. (b) Hydrodynamic diameter of the CuO suspensions with and without SDS during 1 h of resting. (c) Hydrodynamic diameter versus temperature for the nanofluids formed dispersing L/M in ratios of 0.33, 1 and 3, respectively in EG/W (60:40).

However, the reduction rate of aggregation size of the samples prepared with SDS (S2, S4 and S6) was much higher than the ones without surfactants (S1, S3 and S5). As it can be seen in Fig. 7a, after 60 min of ultrasonication cluster sizes of all the samples remained approximately constant. The highest reduction rate of 74 % and the lowest HD corresponded to the sample S2 (with 1.5 wt% of SDS). The reduction rate percentages of the samples S2, S3, S4, S5 and S6 were between 40 % (S3) and 65 % (S6) compared to their cluster sizes before starting the ultrasonication process. These results agree with previous works [28,44,45] in which the ultrasonication period of 60 min improves the stability of the samples. However, raising the time longer than 60 min has been demonstrated to have a negative impact on the nanofluids' stability [44]. Notwithstanding, all the suspensions were stable enough to perform thermal conductivity measurements, as it is shown in Fig. 7b, in which the particle diameters remain constant for at least 1 h. This ensured good conditions to record thermal conductivity measures. The effect of temperature on HD was also investigated. Fig. 7c shows an increase of the HD at 40 °C. This is due to the change in the critical micellar concentration (CMC) at this temperature [46].

The SDS is an anionic surfactant containing polar head (hydrophilic) and non-polar tail (hydrophobic). The repulsive force of the surfactant hydrophobic tail with the ions of the liquid phase enables the adsorption of the SDS molecules onto the CuO nanoparticle surface leading to the creation of a protective layer around the NPs. Meanwhile, the SDS hydrophilic head is in contact with the more polar base fluid reducing the interfacial tension at the solid/liquid interface. The association NP-SDS reduces the free energy, which improves the dispersion stability [33,47]. Through electrostatic repulsions between negatively charged head groups of SDS molecules, the protective layer forms a repulsive barrier, preventing particle aggregation and maintaining nanoparticle

dispersion and the stability in the suspension. A sketch of this mechanism can be represented in Fig. 8. The powder L/M = 0.33 has exhibited the lowest particle size (27.5 nm) and HD = 81 nm at 20 °C (see Fig. 7a). It is because the SDS was adsorbed onto a great part of the particle surface. The electrostatic repulsions prevent any other charged particle from approaching to form a larger cluster. The two other powders, L/M = 1 and L/M = 3 presented particle size of 30.8 nm and 36.7 nm, respectively, and HD of 140 nm, and 200 nm, respectively, at 20 °C with 1.5 wt% of SDS. This increase of the HD could be explained because the surface to be covered by surfactant molecules increased in the L/M = 1 and L/M = 3 powders. As it can be seen in Fig. 7a L/M = 1 and L/M = 3 aggregates have higher HD than L/M = 1. In this case, the smaller surface areas of the last two powders diminished the effectiveness of the surfactant molecules due to the decrease of the surface free energy, as a result the surfactants aggregates formed micelles and lose their efficiency as stabilizers [47]. A possible mechanism of the surfactant action is shown in Fig. 8. As it is represented in this Figure, the electrostatic repulsions diminish and other particles could approach and generate larger aggregates. If the SDS concentration is raised above 1.5 wt%, which is over the critical micellar concentration [46], more micelles are expected to be formed. In this case, the liquid phase appeared foamier and the DLS measures were not credible. In summary, although both surfactant and ultrasonication time are required to produce stable nanofluids, surfactant was considered dominant over ultrasonication.

3.3.2. Sedimentation test

Recently, the sedimentation test has been considered as the most useful, low cost and effective approach [29,30,48]. Sedimentation refers to the tendency of nanoparticles to aggregate in a dispersed base fluid. When gravity dominates over external forces, settling down happens with the creation of nanoparticle aggregates in the bottom of a transparent glass bottle. If the concentration of the dispersed nanoparticles in

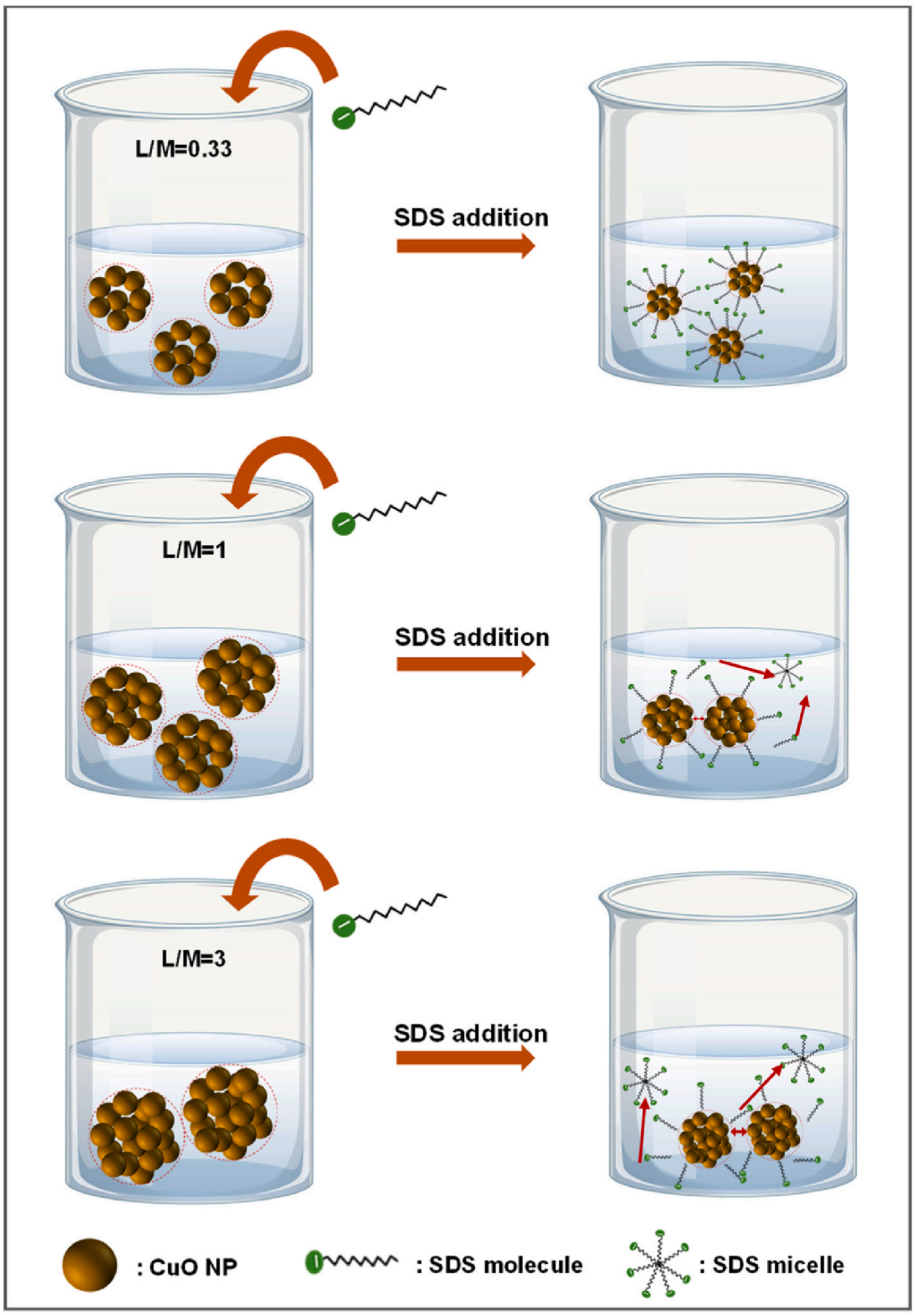

Fig. 8. Schematic representation of the microstructures in the three powders when SDS is added to the liquid phase.

a base fluid remains constant over a defined period the nanofluid can be regarded as stable [48]. To determine the stability of the nanofluids using the sedimentation test, photographs of the samples in glass bottles were captured using a camera. They were observed for 30 days and compared to each other. To visually evaluate the effect of the surfactant on the stability of nanofluids the sedimentation method was performed with and without SDS surfactant. Fig. 9 illustrates the sedimentation pattern of the samples over time. Sample S3 remained stable for only 2 days and the sample S5 for only 1 day. After 5 days, samples S4 and S6 revealed significant sedimentation. However, samples S1 and S2 exhibited the best stability, with negligible sedimentation even after 30 days. The sedimentation test showed that adding of SDS surfactant can significantly increase the stability of nanofluids. Albeit it was assumed that the stability of any dispersion never reaches a long-term development, sample S2 has shown to be stable for more than a week with the addition of the 1.5 wt% SDS surfactant. However, samples S4 and S6, with higher particle size, 140 and 200 nm (measured by DLS), respectively, did not exhibit the same stability as the sample S2 of around 100 nm in suspension. As a result of the difference in the average particle size of the biosynthesized CuO nanoparticles with different L/M ratio, shown in the TEM images (see Fig. 6), the duration the nanoparticles remained suspended was reduced [44,48]. Therefore, it could be inferred that the L/M = 0.33 ratio produced a more disaggregated powder with better quality as nanofluid for heat transfer applications.

3.3.3. *Effect of surfactant on zeta potential*

The zeta potential of the three suspensions S2, S4 and S6 was also measured. Suspensions with zeta potentials lower than 30 mV are considered to have limited stability, from 30 mV to 60 mV good stability, and dispersions with zeta potentials exceeding 60 mV are considered to have excellent stability [15,28]. As it is shown in Fig. 10b, zeta potential analysis indicates that the CuO nanofluids stabilized by SDS surfactant and the ones with lower L/M ratio have better stability. The highest zeta potential value, -61.2 ± 0.9 mV, was observed for the sample L/M = 0.33, 1.5 wt% SDS (S2) at 20 °C and the lowest zeta potential, -34.7 ± 1.1 mV, for the sample L/M = 3, 1.5 wt% SDS (S6) at 60 °C**.** Increasing L/M ratio from 0.33 to 3 resulted in a decrease in the value of zeta potential, which means lower stability. These results could be related to the hydrodynamic diameter of the CuO nanofluids, shown in Fig. 7a higher L/M ratio led to a higher HD and the presence of SDS provided a smaller HD. Thus, it can be concluded that L/M = 0.33 with 1.5 wt% SDS were the optimum conditions in which the best stability can be achieved for the studies of CuO-based nanofluid dispersed in EG/W 60:40. The reduction of the zeta potential at higher temperatures can be caused by the reduction of the suspension viscosity at higher temperatures. According to the Helmholtz- Smoluchowski equation, zeta potential, ζ, and

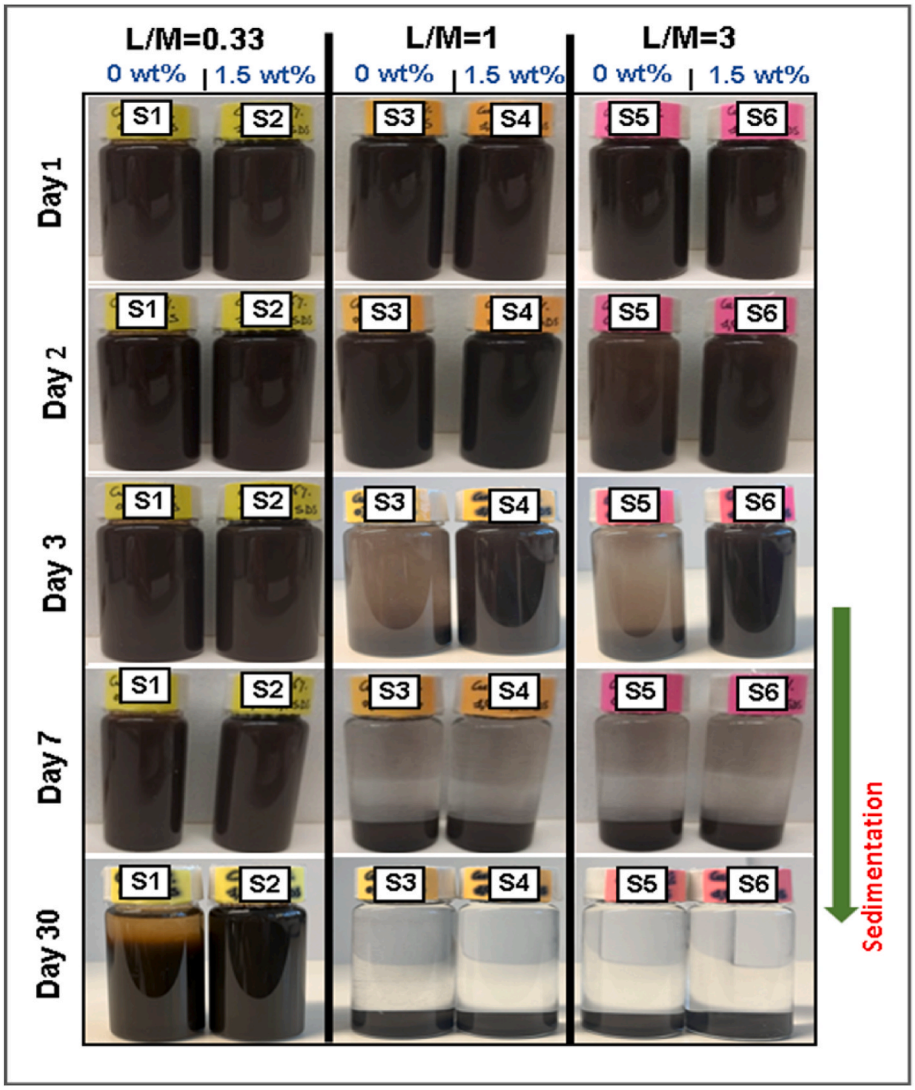

Fig. 9. Samples of CuO based nanofluids with and without SDS with varying L/M ratio (a) immediately after preparation, (b) after 2 days, (c) after 3 days, (d) after 7 days, and (e) after 30 days.

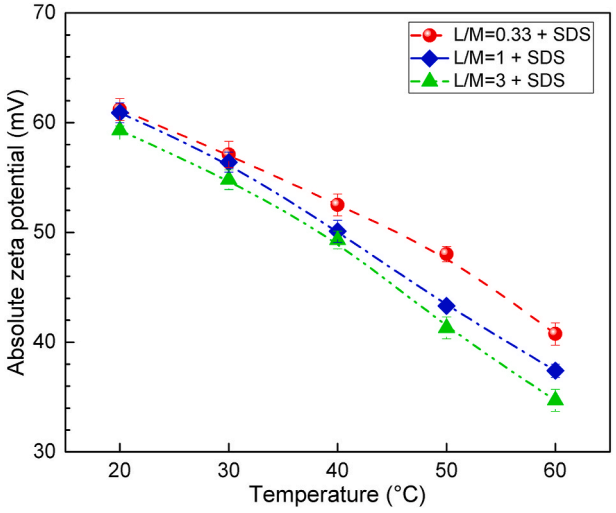

Fig. 10. Absolute zeta potential of CuO based EG/W (60:40 v/v) nanofluids with 1.5 wt% SDS.

electrophoretic mobility, u_e, are related as $u_e = \frac{\varepsilon_r \varepsilon_0}{\eta}\zeta$. Therefore, the electrophoretic mobility increased with temperature while zeta potential reduced with temperature, as it is reported by other researchers [19, 49].

3.4. Thermal conductivity analysis of CuO nanofluids

Fig. 11 shows the experimental thermal conductivity vs. temperature of the three CuO nanopowders (L/M ratios: 0.33, 1 and 3) in concentration of 0.2 vol% dispersed in EG/W 60:40 with 1.5 wt% of SDS. The experimental thermal conductivities of the liquid phase agreed with the values reported by ASHRAE standards [50]. For all the temperatures, it can be appreciated in this figure that the nanofluid prepared with the smaller amount of lemon juice (L/M = 0.33) exhibits higher TC than the other two dispersions. As it is observed in this figure, for the three samples, k_{eff} increases linearly with temperature [19]. Between 20 °C and 60 °C, the TC of the sample's L/M = 0.33, L/M = 1 and L/M = 3 rose by 20.8 %, 22.2 % and 21.9 %, respectively, which suggested that the slope of the three lines was very similar. At 60 °C, the k_{eff} enhancement respect to the based fluid (EG/W 60:40) was 22.8 % for L/M = 0.33 versus 21.7 % for L/M = 1 and 20.4 % for L/M = 3. In contrast with the

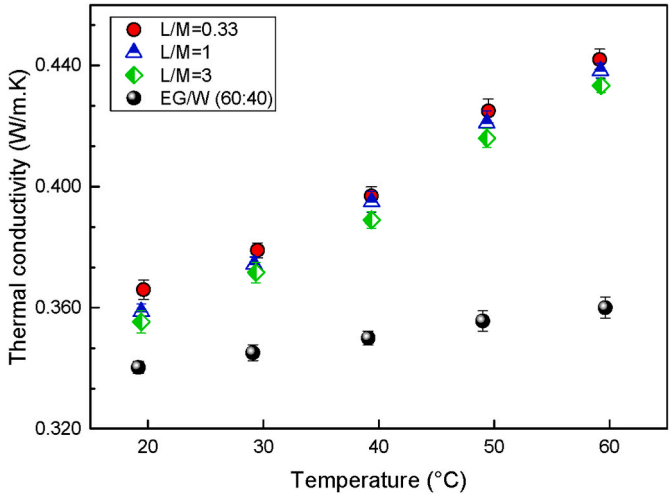

Fig. 11. Thermal conductivity of CuO based EG/W 60:40 nanofluids at a volume concentration of 0.2 % with the presence of 1.5 wt% of the surfactant SDS as a function of temperature. All the uncertainties are under 1 %.

lower values of the k_{eff} enhancement measured at 20 °C, which was 7.5 % for L/M = 0.33, 5.4 % for L/M = 1 and 4.4 % for L/M = 3, respectively. For all the temperatures, it can be inferred that the smaller the particle size the greater the k_{eff}. Albeit the diameter of the single particles synthesized with three proportions of lemon juice (L/M = 0.33, L/M = 1, L/M = 3), see Fig. 6, were between 27 and 37 nm, the formation of aggregates in the respective suspensions of the three powders in EG/W 60:40 with 1.5 wt% of SDS after 60 min of sonication achieved diameters at 20 °C between 100 and 200 nm, as it is represented in Fig. 7. The results of k_{eff} shown in Fig. 11 are meaningful because they were recorded under the same standard conditions and they can be comparable. They confirm the conclusions reported in the literature [18, 51] and reinforce the inverse relationship between k_{eff}, particle size and hydrodynamic diameter found for these researchers. This fact is explained because smaller particles, when present at an equivalent volume concentration, offer a larger surface area than greater particles, thereby enhancing the facilitation of thermal energy transfer, which depends on the surface area of particles [18,19]. However, the k_{eff} enhancement from 20 °C to 60 °C was similar in the three samples, as it was mentioned before. Nonetheless, the higher values of TC were registered for the smaller aggregate sizes, L/M = 0.33. It is believed that the Brownian motion could facilitate other mechanisms of heat transmission due to the greater complexity of particle-base fluid molecule interactions caused by the rising temperature. The base fluid molecules could form ordered layers around each particle, which create a microconvection effect [52]. Another possibility that could occur in response to more collisions of the base fluid molecules with temperature should be the formation or breakdown of particle aggregates [19,53].

The Hamilton-Crosser thermal conductivity theory for nanofluids does not contemplate particle or aggregate size and it reduces to the Maxwell-Garnett theory for spherical particles. However, Fig. 11 reveals that particle and cluster sizes affect the suspension thermal conductivities since the smaller particle and cluster sizes, corresponding to the L/M = 0.33 dispersion, exhibited the higher k_{eff}. To obtain numerical evidence of the particle diameter and cluster size effects, two thermal conductivity theories, which include the influence of solvation nanolayer [26] and liquid layering together with cluster formation effects [27] were tested. The theory proposed by Leong et al. (L) [26] assumes the influence on k_{eff} of the particle size and an interfacial layer surrounding particles. If the liquid phase contains wetting agents, the adsorption of completely extended surfactant molecules onto the particle or cluster surface forms a liquid layering of width δ encircling the CuO species, as it is outlined in Fig. 12. Simultaneously, since particle clusters are bordered by surfactant ions the aggregate radius, r_a, could be regarded as the equivalent to the particle size in this model. The value k_L of the nanofluid thermal conductivity, according to the Leong model, is given by Eq. (1), as follows:

$$k_L = \frac{(k_p - k_{il})\varnothing k_{il}(2\beta_1^3 - \beta^3 + 1) + (k_p + 2k_{il})\beta_1^3[\varnothing\beta^3(k_{il} - k_f) + k_f]}{(k_p + 2k_{il})\beta_1^3 - (k_p - k_{il})\varnothing(\beta_1^3 + \beta^3 - 1)} \quad (1)$$

Notice that Eq. (1) is not applicable at any temperature. It relates k_{eff} with particle concentration, ϕ, as independent variable, at room temperature. The parameters of Eq. (1) are defined as: k_f, the thermal conductivity of the base fluid [50]; k_p = 33 W/m·K, the thermal conductivity of the CuO [54]; k_{il}, the thermal conductivity of the liquid layer, $k_{il} = 2.5 \cdot k_f$; $\beta = 1 + \frac{\delta}{r_a}$; $\beta_1 = 1 + \frac{\delta}{2r_a}$; δ, the thickness of the liquid layer surrounding the particle aggregates, in this study, the value taken was 6 nm, the width of the SDS surfactant molecules [55]; and r_a the cluster radius, as drawn in Fig. 12.

The approach proposed by Machrafi and Lebon (M-L) [27] reflects Brownian motion, liquid layering and agglomerate effects. It also supposes constant temperature (around 20 °C), no charges, spherical particles and the absence of surfactants. Nevertheless, as it was performed in the Leong model, it could be applied with surfactants with the same thickness, δ, as the above-mentioned model. The equation is as follows:

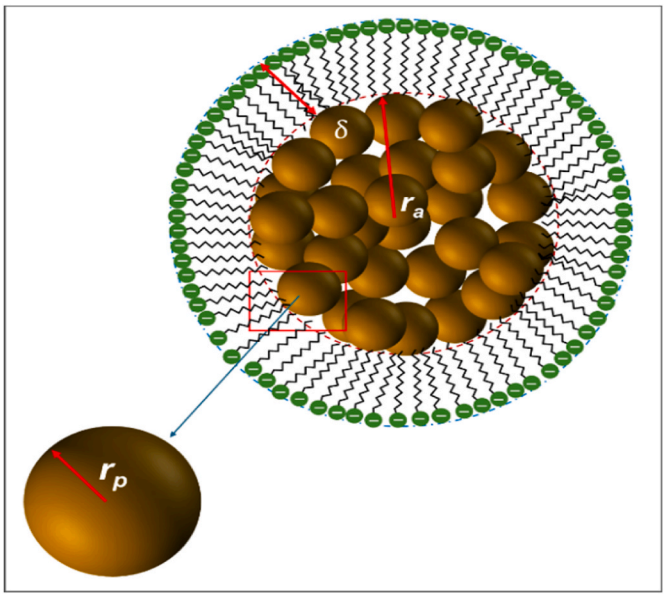

Fig. 12. Graphical representation of a cluster surrounded by surfactant molecules. The parameters used in the two theoretical models checked in Fig. 13 are also outlined.

$$k_{M-L} = k_f \frac{2k_f + (1+2\alpha_a)k_{a,l} + 2\varnothing_a(1+\beta_a)^3\left[(1-\alpha_a)k_{a,l} - k_f\right]}{2k_f + (1+2\alpha_a)k_{a,l} - \varnothing_a(1+\beta_a)^3\left[(1-\alpha_a)k_{a,l} - k_f\right]} \quad (2)$$

The new parameters of Eq. (2) are defined as: $\alpha_a = \frac{R \cdot k_f}{r_a+\delta}$; $\beta_a = \frac{\delta}{r_a}$; $\phi_a = \phi\left(\frac{r_a}{r_p}\right)^{3-D}$; the particle radius, r_p, and the aggregate radius, r_a, were estimated by TEM and DLS whose values at distinct temperatures are shown in Fig. 6(a and b,c) and Fig. 7a. R is the boundary thermal resistance, which depends on the base fluid nature and could vary with temperature. The values of R applied in Eq. (2) were taken from those reported in Ref. [56] for propylene glycol/water 60:40. D is the aggregate fractal dimension whose value taken was 1.78 [62]. The parameter $k_{a,l}$ is calculated by means of Eq. (3).

$$k_{a,l} = \frac{1}{4}\left[3\varnothing_s(k_p - k_f) + (2k_f - k_p) + \sqrt{8k_fk_p + (3\varnothing_s(k_f - k_p) + (k_p - 2k_f))^2}\right] \quad (3)$$

Where $\phi_s = \frac{\phi}{\phi_a}$ is the ratio between particle and aggregate volume fractions, respectively. The theoretical values of the relative thermal conductivity 0.2 vol% CuO dispersed in EG/W 60:40 estimated by means of Eqs. (1) and (2) at various temperatures are depicted in Fig. 13, utilizing a 3D bar chart for enhanced visualization. As it can be appreciated in this Figure, both models predicted very close TC values for the three samples and fitted well the experimental data at 20 °C. It is noteworthy that in both theories the nanofluids with the L/M = 0.33 ratio exhibited higher TC thermal conductivity compared to the nanofluids prepared with the powders synthesized with higher quantities of lemon juice, L/M = 1 and L/M = 3. Fig. 13 also shows the evidence of the low sensitivity of the TC to temperature variations across all L/M ratios for the two theoretical models, Leong (L) and Machrafi-Lebon (M-L). This is due to the initial hypothesis of no dependence on temperature of these two models. The M-L model includes Brownian motion, solvation layer of ordered liquid molecules around particles and cluster formation as possible heat transmission mechanisms while the Leong (L) theory only involves a liquid layering formation as heat transfer mechanism. Since the liquid layering surrounding particle aggregates was estimated as the length of the SDS surfactant molecules for both models and it was used the aggregate radius instead of particle radius in the Leong theory both models converge to close values of thermal conductivities confirming the dominant influence of liquid layering and particle clustering as the more predominant heat exchange mechanisms in these nanofluids. Additionally, to clarify Fig. 13, the deviation suffered by Eqs. (1) and (2) respect to the experimental data was calculated. Thus, the rightness of the two theoretical models to predict TC in CuO nanofluids was assessed. The following Eq. (4) was employed to calculate the percentage of deviation:

$$\%\ of\ deviation = \left[\frac{k_{exp.} - k_{th}}{k_{exp.}}\right] * 100 \quad (4)$$

Table 1 presents the deviations of the two mathematical models with respect to the experimental data. It is seen how at 20 °C, at which the models are designed, the experimental data fit the mathematical values with deviations under 5 %. The k_{eff} of the samples L/M = 1 and L/M = 3 are closer to the experimental thermal conductivities than the L/M = 0.33 powder since the two models underestimate the experimental values of TC. From Eqs. (1) and (2) it could be inferred that, for the same thickness of the liquid layer, higher r_a lead to lower values of k_{eff}. As it can be appreciated in Table 1, the higher the temperature the greater the deviation with respect to the experimental values but the tendency with temperature is the same in all cases. The linear adjustment of the TC with temperature was also performed. The corresponding R^2 coefficients of the experimental and theoretical values were also expressed in Table 1. Apart from the dependency of thermal conductivity with the

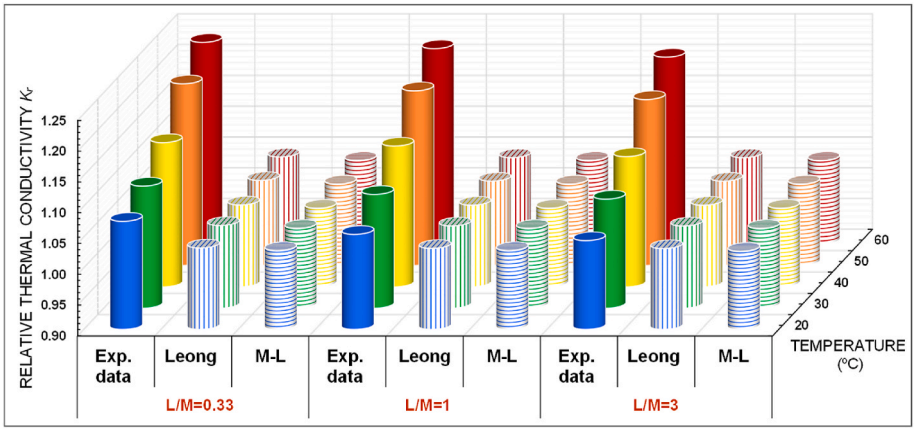

Fig. 13. 3D thermal conductivity changes versus temperature and green fuel ratio of CuO nanoparticles in EG/W 60:40 (v/v) at 0.2 vol%. The uncertainty of the relative thermal conductivity measurements is estimated to be ±5 %. (For interpretation of the references to colour in this figure legend, the reader is referred to the Web version of this article.)

Table 1
Relative thermal conductivity deviations with respect to the experimental data of the two mathematical models. R^2 values of the linear fit of TC versus temperature.

Samples	*Models*	*% Deviation respect to experimental data*						
		20 °C	*30 °C*	*40 °C*	*50 °C*	*60 °C*	$\overline{R^2}$	$\overline{R^2_{Exp}}$
L/M = 0.33	M-L	4.4	6.2	9.4	13.6	15.6	0.99089	0.96979
	Leong	4.0	5.8	8.9	13.1	15.1	0.99743	
L/M = 1	M-L	2.5	5.1	8.9	12.8	14.9	0.99011	
	Leong	2.1	4.7	8.5	12.4	14.5	0.99852	0.98846
L/M = 3	M-L	1.6	4.4	7.5	11.7	13.9	0.99111	0.98544
	Leong	1.2	4.0	7.1	11.3	13.5	0.99832	

nanofluid particle and aggregate size it is also intricately linked to its stability. The addition of SDS contributed to the enhancement of the stability of CuO-based nanofluids, potentially accounting for the observed improvement in the relative TC illustrated in Fig. 13.

4. Conclusions

In the green synthesis of CuO NPs using lemon juice and Cu $(NO3)_2.3H_2O$ in the three L/M (0.33, 1 and 3) ratios the main conclusions are summarized as follows:

The characterization techniques of the three powders through TEM showed an increase of the particle diameter, d_p, with the amount of lemon juice added in the synthesis process. The values of the d_p were 27 nm, 31 nm and 37 nm corresponding to the ratio's L/M = 0.33, L/M = 1 and L/M = 3, respectively. The L/M = 0.33 TEM images exhibited a more disaggregated powder and the EDX showed fewer K and P atoms as impurities.

Ultrasonication time was effective in particle size reduction until an optimal value of 60 min beyond which no significant d_p reduction was observed. At 20 °C, DLS measurements of the three powders dispersed in EG/W (60:40) after 1h of sonication with SDS 1.5 wt% showed particle diameters of 80.6 ± 0.2 nm, 140 ± 5 nm and 196 ± 7 nm for the three L/M ratios (0.33, 1 and 3), respectively, which supposed a reduction ratio of 3.5, 3.1 and 2.2. While the zeta potential yielded optimal values of −61.2 ± 0.9 mV, −60.8 ± 0.7 mV and −59.6 ± 0.4 mV, which showed a significant improvement of the stability and quality of the nanofluids.

The thermal conductivity studies of the three powders revealed an enhancement of the k_{eff} compared to the base fluid. It was also verified an increase in TC when rising temperature. The L/M = 0.33 nanofluids demonstrated the highest TC improvement of 7.5 % vs. 5.4 % for L/M = 1 and 4.4 % for L/M = 3 nanofluids, all of them at 20 °C, 0.02 vol% and1.5 wt% of SDS. In the three samples, the TC raised linearly with temperature. The experimental data of k_{eff} were compared with two thermal conductivity mathematical models, which mainly examine the influence of cluster formation and liquid layering organization around particles. In the two models the DLS measurements of the aggregate diameter was applied. In all cases, the deviation with respect to the experimental values was under 5 % at 20 °C. This good agreement confirmed particle clustering as the heat transfer mechanism which better justified the TC enhancement of the CuO nanofluids. Further research about the effect of particle concentration on TC and viscosity is suggested to comprehensively understand the impact of CuO nanoparticle morphology on thermophysical properties in the context of heat transfer applications.

CRediT authorship contribution statement

Meriem Jebali: Writing – review & editing, Writing – original draft, Visualization, Methodology, Investigation, Formal analysis, Data curation, Conceptualization. **Ana Isabel Gómez-Merino:** Writing – review & editing, Writing – original draft, Supervision, Methodology, Formal analysis, Data curation, Conceptualization. **Gianpiero Colangelo:** Writing – review & editing, Validation, Supervision, Resources, Methodology, Conceptualization.

Declaration of competing interest

The authors declare that they have no known competing financial interests or personal relationships that could have appeared to influence the work reported in this paper.

Acknowledgements

Funding for open access charge: Universidad de Málaga/CBUA. The authors would like to acknowledge Prof. Imene Bekri-Abbes and the National Center for Research in Material Sciences, Technopole of Borj Cedria, Tunisia. The financial support from the Junta de Andalucia, Spain, (PROYEXCEL_00181). The IMECH and the SCAI service of the University of Málaga for the SEM,TEM images and all the CuO characterization spectra.

Nomenclature

d	Diameter (nm)
D	Fractal dimension
k	Thermal conductivity (W/m.K)
r	Radius (nm)
R	Thermal resistance (K/W)
vol	Volume
wt	Weight fraction
ζ	Zeta potential (mV)
η	Viscosity (Pa.s)
ρ	Density (kg/m3)
ϕ	Volume fraction
δ	Thickness of the liquid layer (nm)
u_e	Electrophoretic mobility (μm·cm/V·s)

Susbcripts

a	Aggregate
bf,s	Base fluid, solid
exp.	Experimental
eff	Effective
f	Base fluid
i	Interface
il	Interface layer
L	Leong
M-L	Machrafi-Lebon
nf	Nanofluid
p	Particle
r	Relative
sn	Sonication
th	Theoretical Model

Acronyms

ASHRAE	American Society of Heating, Refrigeration and Air Conditioning Engineers
CMC	Critical micellar concentration
DLS	Dynamic light scattering
DTA	Differential thermal analysis

EG/W	Ethylene glycol/Water
FT-IR	Fourier Transform Infrared
HAADF	High-angle annular dark-field
HD	Hydrodynamic diameter (nm)
L/M	Lemon juice/Metal precursor
LJ	Lemon Juice
SDS	Sodium dodecyl sulfate
SEM	Scanning electron microscopy
TEM	Transmission electron microscopy
TGA	Thermogravimetric analysis
THW	Transient hot wire
X-EDS	Energy dispersive X-ray spectroscopy
XPS	X-ray Photo-correlation Spectroscopy
XRD	X-ray diffraction

References

[1] J.A. Kumar, T. Krithiga, S. Manigandan, S. Sathish, A.A. Renita, P. Prakash, B.S. N. Prasad, T.R.P. Kumar, M. Rajasimman, A. Hosseini-Bandegharaei, D. Prabu, S. Crispin, A focus to green synthesis of metal/metal based oxide nanoparticles: various mechanisms and applications towards ecological approach, J. Clean. Prod. 324 (2021) 129198, https://doi.org/10.1016/j.jclepro.2021.129198.

[2] S. Ying, Z. Guan, P.C. Ofoegbu, P. Clubb, C. Rico, F. He, J. Hong, Green synthesis of nanoparticles: current developments and limitations, Environ. Technol. Innov. 26 (2022) 102336, https://doi.org/10.1016/j.eti.2022.102336.

[3] A. Gour, N.K. Jain, Advances in green synthesis of nanoparticles, Artif. Cell. Nanomed, Biotechnol. 47 (2019) 844–851, https://doi.org/10.1080/21691401.2019.1577878.

[4] K.G. Devi, A.C. Dhanemozhi, L.S. Priya, Green synthesis of Zinc oxide nanoparticles using lemon extract for waste water treatment, Mater. Today: Proc. (2023) 576, https://doi.org/10.1016/j.matpr.2023.03.576.

[5] R.V. Poonguzhali, E.R. Kumar, M.G. Sumithra, N. Arunadevi, C.S. Rahale, A. M. Munshi, G.A.M. Mersal, N.M. El-metwaly, Natural citric acid (lemon juice) assisted synthesis of ZnO nanostructures: evaluation of phase composition, morphology, optical and thermal properties, Ceram. Int. 47 (2021) 23110–23115, https://doi.org/10.1016/j.ceramint.2021.05.024.

[6] R. Jothiramalingam, S. Devasanan, M.R. Muthumareeswaran, H.M. Alqahtani, K. Abdalnaser, Green chemistry method prepared effective copper nanoparticles by lemon flower (citrus) extract and its anti-microbial activity, Dig. J. Nanomater. Biostruct. 17 (2022) 145–151, https://doi.org/10.15251/DJNB.2022.171.145.

[7] B. Murugan, M.Z. Rahman, I. Fatimah, J. Anita Lett, J. Annaraj, N.H.M. Kaus, M. A. Al-Anber, S. Sagadevan, Green synthesis of CuO nanoparticles for biological applications, Inorg. Chem. Commun. 155 (2023) 111088, https://doi.org/10.1016/j.inoche.2023.111088.

[8] P.G. Bhavyasree, T.S. Xavier, Green synthesised copper and copper oxide based nanomaterials using plant extracts and their application in antimicrobial activity: review, Curr. Res. Green Sustain. Chem. 5 (2022) 100249, https://doi.org/10.1016/j.crgsc.2021.100249.

[9] N. Chakraborty, J. Banerjee, P. Chakraborty, S. Chanda, K. Ray, K. Acharya, J. Sarkar, Green Chemistry Letters and Reviews Green synthesis of copper/copper oxide nanoparticles and their applications : a review, Green Chem. Lett. Rev. 15 (2022) 187–215, https://doi.org/10.1080/17518253.2022.2025916.

[10] I. Kir, H.A. Mohammed, S.E. Laouini, M. Souhaila, G.G. Hasan, Plant extract - mediated synthesis of CuO nanoparticles from lemon peel extract and their modification with polyethylene glycol for enhancing photocatalytic and antioxidant activities, J. Polym. Environ. 32 (2023) 718–734, https://doi.org/10.1007/s10924-023-02976-x.

[11] J. Vincent, K.S. Lau, Y.C.Y. Evyan, S.X. Chin, M. Sillanpää, C.H. Chia, Biogenic synthesis of copper-based nanomaterials using plant extracts and their applications: current and future directions, Nanomaterials 12 (2022) 3312, https://doi.org/10.3390/nano12193312.

[12] M. Amer, A. Awwad, Green synthesis of copper nanoparticles by Citrus limon fruits extract, characterization and antibacterial activity, Chem. Int. 7 (2021) 1–8.

[13] S. Mohan, Y. Singh, D.K. Verma, S.H. Hasan, Synthesis of CuO nanoparticles through green route using Citrus limon juice and its application as nanosorbent for Cr(VI) remediation: process optimization with RSM and ANN-GA based model, Process Saf. Environ. Prot. 96 (2015) 156–166, https://doi.org/10.1016/j.psep.2015.05.005.

[14] A. Waris, M. Din, A. Ali, M. Ali, S. Afridi, A. Baset, A. Ullah Khan, A comprehensive review of green synthesis of copper oxide nanoparticles and their diverse biomedical applications, Inorg. Chem. Commun. 123 (2021) 108369, https://doi.org/10.1016/j.inoche.2020.108369.

[15] C.A. Paul, E.R. Kumar, J. Suryakanth, A.F. Abd El-Rehim, Analysis and characterization of structural, morphological, thermal properties and colloidal stability of CuO nanoparticles for various natural fuels, Ceram. Inter. 49 (2023) 31193–31209, https://doi.org/10.1016/j.ceramint.2023.07.065.

[16] F. Ansari, M. Salavati-Niasari, Simple sol-gel auto-combustion synthesis and characterization of lead hexaferrite by utilizing cherry juice as a novel fuel and green capping agent, Adv. Powder Technol. 27 (2016) 2025–2031, https://doi.org/10.1016/j.apt.2016.07.011.

[17] G. Colangelo, E. Favale, P. Miglietta, M. Milanese, A. de Risi, Thermal conductivity, viscosity and stability of Al_2O_3-diathermic oil nanofluids for solar energy systems, Energy 95 (2016) 124–136, https://doi.org/10.1016/j.energy.2015.11.032.

[18] T. Ambreen, M. Kim, Influence of particle size on the effective thermal conductivity of nanofluids : a critical review, Appl. Energy 264 (2020) 114684, https://doi.org/10.1016/j.apenergy.2020.114684.

[19] S. Porgar, H.F. Oztop, S. Salehfekr, A comprehensive review on thermal conductivity and viscosity of nanofluids and their application in heat exchangers, J. Mol. Liq. 386 (2023) 122213, https://doi.org/10.1016/j.molliq.2023.122213.

[20] P.B. Maheshwary, C.C. Handa, K.R. Nemade, A comprehensive study of effect of concentration, particle size and particle shape on thermal conductivity of titania/water based nanofluid, Appl. Therm. Eng. 119 (2017) 79–88, https://doi.org/10.1016/j.applthermaleng.2017.03.054.

[21] E.V. Timofeeva, J.L. Routbort, D. Singh, Particle shape effects on thermophysical properties of alumina nanofluids, J. Appl. Phys. 106 (2009) 014304, https://doi.org/10.1063/1.3155999.

[22] E. Marín, A. Bedoya, S. Alvarado, A. Calderón, R. Ivanov, F. Gordillo-Delgado, An explanation for anomalous thermal conductivity behaviour in nanofluids as measured using the hot-wire technique, J. Phys. D Appl. Phys. 47 (2014) 085501, https://doi.org/10.1088/0022-3727/47/8/085501.

[23] F. Iacobazzi, M. Milanese, G. Colangelo, M. Lomascolo, A. de Risi, An explanation of the Al_2O_3 nanofluid thermal conductivity based on the phonon theory of liquid, Energy 116 (2016) 786–794, https://doi.org/10.1016/j.energy.2016.10.027.

[24] M. Milanese, F. Iacobazzi, G. Colangelo, A. de Risi, An investigation of layering phenomenon at the liquid–solid interface in Cu and CuO based nanofluids, Int. J. Heat Mass Transf. 103 (2016) 564–571, https://doi.org/10.1016/j.ijheatmasstransfer.2016.07.082.

[25] F. Iacobazzi, M. Milanese, G. Colangelo, A. de Risi, A critical analysis of clustering phenomenon in Al_2O_3 nanofluids, J. Therm. Anal. Calorim. 135 (2019) 371–377, https://doi.org/10.1007/s10973-018-7099-9.

[26] K.C. Leong, C. Yang, S.M.S. Murshed, A model for the thermal conductivity of nanofluids - the effect of interfacial layer, J. Nanopart. Res. 8 (2006) 245–254, https://doi.org/10.1007/s11051-005-9018-9.

[27] H. Machrafi, G. Lebon, The role of several heat transfer mechanisms on the enhancement of thermal conductivity in nanofluids, Continuum Mech. Thermodyn. 28 (2016) 1461–1475, https://doi.org/10.1007/s00161-015-0488-4.

[28] S. Chakraborty, P.K. Panigrahi, Stability of nanofluid: a review, Appl. Therm. Eng. 174 (2020) 115259, https://doi.org/10.1016/j.applthermaleng.2020.115259.

[29] A.A. Albert, D.G. Harris Samuel, V. Parthasarathy, Review of stability enhanced nanofluids prepared by one-step methods—heat transfer mechanism and thermo-physical properties, Chem. Eng. Commun. 210 (2023) 1822–1852. https://10.1080/00986445.2022.2147833.

[30] K.S. Pavithra, Fasiulla, M.P. Yashoda, S. Prasannakumar, Synthesis, characterisation and thermal conductivity of CuO - water based nanofluids with different dispersants, Part, Sci. Technol. 38 (2019) 1–9, https://doi.org/10.1080/02726351.2019.1574941.

[31] V. Arasu, D. Kumar, I. Khan, Experimental investigation of thermal conductivity and stability of TiO_2-Ag/water nanocomposite fluid with SDBS and SDS surfactants, Thermochim. Acta 678 (2019) 178308, https://doi.org/10.1016/j.tca.2019.178308.

[32] R.V. Poonguzhali, E.R. Kumar, N. Arunadevi, C. Srinivas, M.E. Khalifa, S. Abumelha, N.M. El-metwaly, Natural citric acid assisted synthesis of CuO nanoparticles : evaluation of structural, optical, morphological properties and colloidal stability for gas sensor applications, Ceram. Int. 48 (2022) 26287–26293, https://doi.org/10.1016/j.ceramint.2022.05.311.

[33] A. Kaggwa, J.K. Carson, M. Atkins, M. Walmsley, The effect of surfactants on viscosity and stability of activated carbon, alumina and copper oxide nanofluids, Mater. Today Proc. 18 (2019) 510–519, https://doi.org/10.1016/j.matpr.2019.06.240.

[34] P.R. Ghosh, D. Fawcett, S.B. Sharma, G.E.J. Poinern, Production of high-value nanoparticles via horticultural food waste, Materials 10 (2017) 00852, https://doi.org/10.3390/ma10080852.

[35] F. Buazar, S. Sweidi, M. Badri, F. Kroushawi, Biofabrication of highly pure copper oxide nanoparticles using wheat seed extract and their catalytic activity: a mechanistic approach, Green Process. Synth. 8 (2019) 691–702, https://doi.org/10.1515/gps-2019-0040.

[36] S. Azizi, R. Mohamad, M.M. Shahri, D.J. McPhee, Green microwave-assisted combustion synthesis of zinc oxide nanoparticles with Citrullus colocynthis (L.) schrad: characterization and biomedical applications, Molecules 22 (2017) 1–13, https://doi.org/10.3390/molecules22020301.

[37] W. Zhao, W. Fu, H. Yang, C. Tian, M. Li, Y. Li, L. Zhang, Y. Sui, X. Zhou, H. Chen, G. Zou, Electrodeposition of Cu_2O films and their photoelectrochemical properties, CrystEngComm 13 (2011) 2871–2877, https://doi.org/10.1039/c0ce00829j.

[38] N. Habbache, N. Alane, S. Djerad, L. Tifouti, Leaching of copper oxide with different acid solutions, Chem. Eng. J. 152 (2009) 503–508, https://doi.org/10.1016/j.cej.2009.05.020.

[39] B.T. Sone, A. Diallo, X.G. Fuku, A. Gurib-Fakim, M. Maaza, Biosynthesized CuO nano-platelets: physical properties and enhanced thermal conductivity nanofluidics, Arab. J. Chem. 13 (2020) 160–170, https://doi.org/10.1016/j.arabjc.2017.03.004.

[40] V.U. Siddiqui, A. Ansari, R. Chauhan, W.A. Siddiqi, Green synthesis of copper oxide (CuO) nanoparticles by Punica granatum peel extract, Mater. Today: Proc. 36 (2019) 751–755, https://doi.org/10.1016/j.matpr.2020.05.504.

[41] Z. Ahsani-Namin, R. Norouzbeigi, H. Shayesteh, Green mediated combustion synthesis of copper zinc oxide using Eryngium planum leaf extract as a natural

green fuel: excellent adsorption capacity towards Congo red dye, Ceram. Int. 48 (2022) 20961–20973, https://doi.org/10.1016/j.ceramint.2022.04.090.
[42] L.D. Jadhav, S.P. Patil, A.P. Jamale, A.U. Chavan, Solution combustion synthesis: role of oxidant to fuel ratio on powder properties, Mater. Sci. Forum 757 (2013) 85–98. Trans Tech Publications Ltd, https://doi.org/10.4028/www.scientific.net/MSF.757.85.
[43] N.S. Mane, V. Hemadri, Experimental investigation of stability, properties and thermo-rheological behaviour of water-based hybrid CuO and Fe_3O_4 nanofluids, Int. J. Thermophys. 43 (2022) 1–22, https://doi.org/10.1007/s10765-021-02938-2.
[44] M. Kamalgharibi, F. Hormozi, S.A.H. Zamzamian, M.M. Sarafraz, Experimental studies on the stability of CuO nanoparticles dispersed in different base fluids: influence of stirring, sonication and surface active agents, Heat Mass Transf 52 (2016) 55–62. https://doi10.1007/s00231-015-1618-z.
[45] S.M. Shaban, J. Kang, D.H. Kim, Surfactants: recent advances and their applications, Compos. Commun. 22 (2020) 100537, https://doi.org/10.1016/j.coco.2020.100537.
[46] S.A. Markarian, L.R. Harutyunyan, R.S. Harutyunyan, The properties of mixtures of sodium dodecylsulfate and diethylsulfoxide in water, J. Solution Chem. 34 (2005) 361–368, https://doi.org/10.1007/s10953-005-3056-x.
[47] F. Hakiki, D.A. Maharsi, T. Marhaendrajana, Surfactant-polymer coreflood simulation and uncertainty analysis derived from laboratory study, J. Eng. Technol. Sci. 47 (2015) 706–725, https://doi.org/10.5614/j.eng.technol.sci.2015.47.6.9.
[48] J. Wang, X. Yang, J.J. Klemeš, K. Tian, T. Ma, B. Sunden, A review on nanofluid stability: preparation and application, Renew. Sustain. Energy Rev. 188 (2023) 113854, https://doi.org/10.1016/j.rser.2023.113854.
[49] N. Silva, S. Ramírez, I. Díaz, A. Garcia, N. Hassan, Easy, quick, and reproducible sonochemical synthesis of CuO nanoparticles, Materials 12 (2019) 1–13, https://doi.org/10.3390/MA12050804.
[50] A. Standard, ASHRAE Handbook 2009 Fundamentals, SI Edition, Ashrae, Standard, 2009, pp. 24–25.
[51] R. Agarwal, K. Verma, N.K. Agrawal, R.K. Duchaniya, R. Singh, Synthesis, characterization, thermal conductivity and sensitivity of CuO nanofluids, Appl. Therm. Eng. 102 (2016) 1024–1036, https://doi.org/10.1016/j.applthermaleng.2016.04.051.
[52] C.H. Li, G.P. Peterson, Experimental investigation of temperature and volume fraction variations on the effective thermal conductivity of nanoparticle suspensions (nanofluids), J. Appl. Phys. 99 (2006), https://doi.org/10.1063/1.2191571.
[53] S. Daviran, A. Kasaeian, H. Tahmooressi, A. Rashidi, D. Wen, O. Mahian, Evaluation of clustering role versus Brownian motion effect on the heat conduction in nanofluids: a novel approach, Int. J. Heat Mass Transf. 108 (2017) 822–829, https://doi.org/10.1016/j.ijheatmasstransfer.2016.12.071.
[54] S. Alosious, R. Sarath, A.R. Nair, K. Krishnakumar, Experimental and numerical study on heat transfer enhancement of flat tube radiator using Al_2O_3 and CuO nanofluids, Heat and Mass Transf. 53 (2017) 3545–3563, https://doi.org/10.1007/s00231-017-2061-0.
[55] Y. Mirgorod, A. Chekadanov, T. Dolenko, Structure of micelles of sodium dodecyl sulphate in water: an X-ray and dynamic light scattering study, Chem. J. Mold. 14 (2019) 107–119, https://doi.org/10.19261/cjm.2019.572.
[56] M. Jebali, C. Colangelo, A.I. Gomez-Merino, Green synthesis, characterization, and empirical thermal conductivity assessment of ZnO nanofluids for high-efficiency heat-transfer applications, Materials 16 (2023) 1542, https://doi.org/10.3390/ma16041542.